Lagrangian Properties and Control of Soft Robots Modeled with Discrete Cosserat Rods.

Lekan Molu, Shaoru Chen, and Audrey Sedal

Abstract—The characteristic in-plane bending associated with soft robots' deformation make them preferred over rigid robots in sophisticated manipulation and movement tasks. However, executing such strategies to precision presents modeling and control challenges given the infinite degrees-of-freedom characteristic of soft robots. Assuming *piecewise constant strains* (PCS) across (discretized) Cosserat microsolids on the robot, their dynamics become amenable to tractable mathematical analysis. While this PCS model handles in-plane bending well, its properties are not exploited for control neither is currently any *rigorous study on the dynamic performance* of multisection deformable materials *during in-plane control that guarantees steady-state convergence*. In this sentiment, we first establish the PCS model's structural Lagrangian properties. Second, we exploit these properties for steady-state convergence on various strain goal states. Third, we benchmark our hypotheses against an Octopus-inspired robot arm under different constant tip-loads. These induce non-constant "in-plane" deformation and we regulate strain states throughout the continuum in these configurations. Our numerical results establish convergence to desired equilibrium throughout the continuum in all of our tests. Within the bounds here set, we conjecture that our methods can find wide adoption in the control of cable- and fluid-driven multisection soft robotic arms; and may be extensible to the (learning-based) control of deformable agents employed in simulated, mixed, or augmented reality.

I. INTRODUCTION

Soft robots are attracting wide adoption in the automation community owing to their improved bending, torsion, configurability, and compliance properties. These properties enable customizable solutions for assistive wearable devices [21], [1], robot grippers [11], and mobile robots [12]. In-plane bending, as a motion deformation strategy, is a particular advantage that serial soft arms execute better than rigid arms. With this property, soft robot grippers can pick up delicate objects, adopt adept nonlinear motion strategies in complex workspaces e.g. for reaching tasks. In embodied applications such as soft exogloves [15] and exosuits [13], they provide conformal deformation that aids improved walking gaits, and muscle rehabilitation and they conserve energy economy.

Drs. Lekan Molu and Shaoru Chen are with Microsoft Research NYC. Prof. Audrey Sedal is with McGill University's Department of Mechanical Engineering. Emails: {lekanmolu, shaoru.chen}@microsoft.com, audrey.sedal@mcgill.ca.
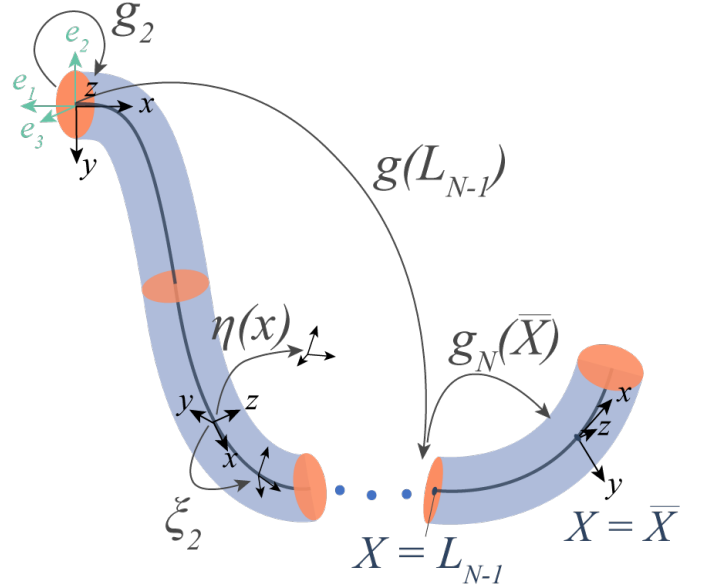
Fig. 1. Schematic of the configuration of an Octopus robot arm.

The piecewise constant strain (PCS) Lagrangian dynamics derived by [17] is a reduced special Euclidean group-3 ($\mathbb{SE}(3)$) model for compliant, serial manipulators. Derived from Cosserat [6] rod theory, it addresses torsion, in-plane, and out-of-plane (multi-) bending motions. The PCS model outperforms the common piecewise constant curvature (PCC) [16] and the constant curvature variants [8] used outside of finite element modeling methods (FEM) [5]. Controllers deployed on the PCS model however ignore the geometric properties of the Lagrangian dynamics [4, 20]. This makes the control equations complicated and destroys several properties of the Lagrangian dynamics that are useful for control tasks.

In this sentiment, considering the PCS model for soft multisection arms, we first establish the structural properties of their Lagrangian dynamics. We then exploit these for the steady-state convergence analyses in various control proposals (under different operating model parameters) and in different surrounding mediums using the well-established method of Lyapunov analysis. The Octopus robot [10] is a testbed on which models and control of soft manipulators can be validated. Therefore, we consider a single arm of this robot (configuration shown in Fig. 1) to benchmark our controllers *on the characteristic difficult-to-model and*

control in-plane bending deformation .

II. NOTATIONS AND PRELIMINARIES

The strain field and strain twist vectors are respectively $\xi \in \mathbb{R}^6$ and $\eta \in \mathbb{R}^6$. The Lie algebra of $\mathbb{SE}(3)$ is $\mathfrak{se}(3)$. All angles are measured counterclockwise. For a configuration $\boldsymbol{g}(X) \in \mathbb{SE}(3)$, its adjoint and coadjoint representations are respectively $\mathrm{Ad}_{\boldsymbol{g}}$, $\mathrm{Ad}_{\boldsymbol{g}}^{\star}$ – parameterized by a curve i.e. the material abscissa X. The corresponding adjoint and coadjoint representation of the strain twist vector are $\mathrm{ad}_{\xi,\eta}$ and $\mathrm{ad}_{\xi,\eta}^{\star}$, respectively. In generalized coordinate, the joint vector of a soft robot is denoted $q(\xi) = [\xi_1^\top, \ldots, \xi_{n_\xi}^\top]^\top \in \mathbb{R}^{6n_\xi}$.

A. SoRo Configuration

The inertial frame is signified by the basis triad $(\boldsymbol{e}_1, \boldsymbol{e}_2, \boldsymbol{e}_3)$ (see Fig. 1) and $\boldsymbol{g}_r(X)$ is the transformation from the inertial to the manipulator's base frame. The continuum is reduced to a space curve defined by a material abscissa $X : [0, L]$, where L is the robot's length in the reference configuration. For cable-driven arms, the point at which actuation occurs is labeled $\bar{X}$. The configuration matrix that parameterizes curve L_n in X is denoted $\boldsymbol{g}_{L_n}$. The cable runs through the z-axis (x-axis in the spatial frame) in the (micro) body frame. As shown in Fig. 1, the transformation from the base to the inertial frame is

$$\boldsymbol{g}_r = \begin{pmatrix} 0 & -1 & 0 & 0 \\ 1 & 0 & 0 & 0 \\ 0 & 0 & 1 & 0 \\ 0 & 0 & 0 & 1 \end{pmatrix}. \tag{1}$$

We adopt a linear viscoelastic constitutive model based on Kelvin-Voight internal forces i.e.

$$\mathcal{F}_i(X) = \Sigma(\xi - \xi_0) + \Upsilon\dot{\xi}, \tag{2}$$

with Σ being the constant screw stiffness matrix, Υ the viscosity matrix, and the reference strain vector $\xi_0 = [0, 0, 0, 1, 0, 0]^\top$ in the upright configuration. The jacobian associated with X is denoted $J(X)$. Owing to paper length reasons we refer readers to its definition in [17].

B. Continuous Strain Vector and Twist Velocity Fields

Let $p(X)$ describe the position vector of a microsolid on a soft body and let $R(X)$ denote the corresponding orientation matrix. Furthermore, let the pose $[p(X), R(X)]$ be parameterized by a material abscissa $X \in [0, L]$ for end nodes 0 and L. Then, the robot's C-space, parameterized by a curve $g(X) : X \to \mathbb{SE}(3)$, is $g(X) = \begin{pmatrix} R(X) & p(X) \\ 0^\top & 1 \end{pmatrix}$. Suppose that $\varepsilon(X) \in \mathbb{R}^3$ and $\gamma(X) \in \mathbb{R}^3$ respectively denote the linear and angular strain components of the soft arm. Then, the arm's strain field is a state vector along the curve $g(X)$ defined as $\breve{\xi}(X) = g^{-1}\partial g/\partial X \triangleq g^{-1}\partial_x g$, and the velocity of $g(X)$ is the twist vector field $\breve{\eta}(X)$ defined as $\breve{\eta}(X) = g^{-1}\partial g/\partial t \triangleq g^{-1}\partial_t g$. Read $\hat{\gamma}$: the anti-symmetric

matrix representation of γ. Read $\breve{\xi}$: the isomorphism mapping the twist vector, $\xi \in \mathbb{R}^6$, to its matrix representation in $\mathfrak{se}(3)$.

C. Discrete Cosserat System: Cosserat-Constitutive PDEs

The PCS model assumes that the respective strain, ξ_i for n microsolid sections, $\mathcal{M}_i$, $i = 1, \ldots, n$, are constant for each discretized section of a soft arm. Using d'Alembert's principle, the generalized dynamics for the PCS model (cf. Fig. 1) under external and actuation loads admits the following weak form representation [17]

$$\underbrace{\left[\int_0^{L_N} J^T \mathcal{M}_a J dX\right]}_{M(q)} \ddot{q} + \underbrace{\left[\int_0^{L_N} J^T \mathrm{ad}_{J\dot{q}}^\star \mathcal{M}_a J dX\right]}_{C_1(q,\dot{q})} \dot{q} +$$

$$\underbrace{\left[\int_0^{L_N} J^T \mathcal{M}_a \dot{J} dX\right]}_{C_2(q,\dot{q})} \dot{q} + \underbrace{\left[\int_0^{L_N} J^T \mathcal{D}J \|J\dot{q}\|_p dX\right]}_{D(q,\dot{q})} \dot{q}$$

$$- (1 - \rho_f/\rho) \underbrace{\left[\int_0^{L_N} J^T \mathcal{M} \mathrm{Ad}_{\boldsymbol{g}}^{-1} dX\right]}_{N(q)} \mathrm{Ad}_{\boldsymbol{g}_r}^{-1}\mathcal{G} - \underbrace{J(\bar{X})^T \mathcal{F}_p}_{F(q)}$$

$$- \underbrace{\int_0^{L_N} J^T \left[\nabla_x \mathcal{F}_i - \nabla_x \mathcal{F}_a + \mathrm{ad}_{\eta_n}^\star (\mathcal{F}_i - \mathcal{F}_a)\right] dX}_{\tau(q)} = 0 \tag{3}$$

where $\mathcal{F}_i(X) \triangleq \left(M_i^T, F_i^T\right)^T \equiv \partial_X \mathfrak{U}$ is the wrench of internal forces, $\bar{\mathcal{F}}_a(X)$ is the *distributed* wrench of actuation loads, and $\bar{\mathcal{F}}_e(X)$ is the external *distributed* wrench of the applied forces. The screw mass inertia matrix is $\mathcal{M}(X) = \mathrm{diag}\left(J_x, J_y, J_z, A, A, A\right)\rho$ for a body density ρ, sectional area A, bending, torsion, and second inertia operator J_x, J_y, J_z respectively. In (3), $\mathcal{M}_a = \mathcal{M} + \mathcal{M}_f$ is a lumped sum of the microsolid mass inertia operator, $\mathcal{M}$, and that of the added mass fluid, $\mathcal{M}_f$; dX is the length of each section of the multi-robot arm; $\mathcal{D}(X)$ is the drag matrix; $J(X)$ is the Jacobian operator; $\|\cdot\|_p$ is the translation norm of the expression contained therein; ρ_f is the density of the fluid in which the material moves; ρ is the body density; $\mathcal{G} = [0, 0, 0, -9.81, 0, 0]^T$ is the gravitational vector; and $\mathcal{F}_p$ is the applied wrench at $\bar{X}$. In standard Newton-Euler form, equation (3), is

$$M(q)\ddot{q} + [C_1(q, \dot{q}) + C_2(q, \dot{q})]\,\dot{q} = \tau(q) + F(q)$$
$$+ N(q)\mathrm{Ad}_{\boldsymbol{g}_r}^{-1}\mathcal{G} - D(q, \dot{q})\dot{q}. \tag{4}$$

III. STRUCTURAL PROPERTIES OF THE PCS MODEL

We now establish the Lagrangian properties.

Theorem 1 (Structural properties of the kinetic equation)**.** *Equation* (4) *satisfies the following properties:*

Property 1 (Positive definiteness of the Inertia Operator). *The inertia tensor $\mathcal{M}_a(q)$ is symmetric and positive definite. As a result $M(q)$ is symmetric and positive definite.*

Proof of Property 1. The jacobian, J, is injective by [17, equation 20]. Thus, property 1 follows from its definition. $\square$

Property 2 (Boundedness of the Mass Matrix). *The mass inertial matrix $M(q)$ is uniformly bounded from below by $m\boldsymbol{I}_n$ where m is a positive constant.*

Proof of Property 2. This is a restatement of the lower boundedness of $M(q)$ for fully actuated n-degrees of freedom manipulators [18]. $\square$

Property 3 (Skew symmetric property). *The matrix $\dot{M}(q) - 2\left[C_1(q,\dot{q}) + C_2(q,\dot{q})\right]$ is skew-symmetric.*

Proof of Property 3. We have by Leibniz's rule that

$$\dot{M}(q) = \frac{d}{dt}\left(\int_0^{L_N} J^T \mathcal{M}_a J dX\right) = \int_0^{L_N} \frac{\partial}{\partial t}\left(J^T \mathcal{M}_a J\right) dX$$
$$\triangleq \int_0^{L_N}\left(\dot{J}^T \mathcal{M}_a J + J^T \dot{\mathcal{M}}_a J + J^T \mathcal{M}_a \dot{J}\right) dX. \tag{5}$$

Therefore, $\dot{M}(q) - 2\left[C_1(q,\dot{q}) + C_2(q,\dot{q})\right]$ can be expanded as

$$\int_0^{L_N}\left(\dot{J}^\top \mathcal{M}_a J + J^\top \dot{\mathcal{M}}_a J + J^\top \mathcal{M}_a \dot{J}\right) dX$$
$$- 2\int_0^{L_N}\left(J^\top \mathrm{ad}^\star_{J\dot{q}} \mathcal{M}_a J + J^\top \mathcal{M}_a \dot{J}\right) dX \tag{6}$$
$$\triangleq \int_0^{L_N}\left(\dot{J}^\top \mathcal{M}_a J + J^\top \dot{\mathcal{M}}_a J - J^\top \mathcal{M}_a \dot{J}\right) dX$$
$$- 2\int_0^{L_N} J^\top \mathrm{ad}^\star_{J\dot{q}} \mathcal{M}_a J dX. \tag{7}$$

Similarly, $-\left[\dot{M}(q) - 2\left[C_1(q,\dot{q}) + C_2(q,\dot{q})\right]\right]^\top$ expands as

$$- \dot{M}^\top(q) + 2\left[C_1^\top(q,\dot{q}) + C_2^\top(q,\dot{q})\right] =$$
$$\int_0^{L_N} dX^\top\left(-J^\top \mathcal{M}_a \dot{J} - J^\top \dot{\mathcal{M}}_a J - \dot{J}^\top \mathcal{M}_a J\right)$$
$$+ 2\int_0^{L_N} dX^\top\left(J^\top \mathcal{M}_a \mathrm{ad}_{J\dot{q}} J + \dot{J}^\top \mathcal{M}_a J\right)$$
$$\triangleq \int_0^{L_N}\left(J^\top \mathcal{M}_a \dot{J} - \dot{J}^\top \mathcal{M}_a J - J^\top \dot{\mathcal{M}}_a J\right) dX$$
$$- 2\int_0^{L_N} J^\top \mathrm{ad}^\star_{J\dot{q}} \mathcal{M}_a J dX \tag{8}$$

where the terms in equation (8) follow from the symmetry of the matrices that constitute the integrands. Inspecting (7)

and (8), it is easy to see that their right hand sides verify the identity

$$\int_0^{L_N}\left(\dot{J}^\top \mathcal{M}_a J + J^\top \dot{\mathcal{M}}_a J - J^\top \mathcal{M}_a \dot{J}\right) dX$$
$$- 2\int_0^{L_N} J^\top \mathrm{ad}^\star_{J\dot{q}} \mathcal{M}_a J dX = 2\int_0^{L_N} J^\top \mathrm{ad}^\star_{J\dot{q}} \mathcal{M}_a J dX -$$
$$\int_0^{L_N}\left(J^\top \mathcal{M}_a \dot{J} - \dot{J}^\top \mathcal{M}_a J - J^\top \dot{\mathcal{M}}_a J\right) dX \tag{9}$$

or

$$\dot{M}(q) - 2\left[C_1(q,\dot{q}) + C_2(q,\dot{q})\right] =$$
$$- \left[\dot{M}(q) - 2\left[C_1(q,\dot{q}) + C_2(q,\dot{q})\right]\right]^\top. \tag{10}$$

A fortiori, the skew symmetric property follows. $\square$

Remark 1. *Since $\dot{M}(q)$ is symmetric (cref. (5)), another way of stating the skew-symmetric property is to write*

$$\dot{M}(q) = C_1(q,\dot{q}) + C_2(q,\dot{q}) + \left[C_1(q,\dot{q}) + C_2(q,\dot{q})\right]^\top. \tag{11}$$

Owing to the symmetry of the right-hand-side (rhs), we have $\dot{M} = 2(C_1 + C_2)$.

Property 4 (Linearity-in-the-parameters). *There exists a constant vector $\Theta \in \mathbb{R}^l$ and an $N \times l$ dimensional regressor function $Y(q,\dot{q},\ddot{q}) \in \mathbb{R}^{N\times l}$ such that*

$$M(q)\ddot{q} + \left[C_1(q,\dot{q}) + C_2(q,\dot{q}) + D(q,\dot{q})\right]\dot{q} - F(q) -$$
$$+ N(q)Ad^{-1}_{\boldsymbol{g}_r}\mathcal{G} = Y(q,\dot{q},\ddot{q})\Theta. \tag{12}$$

Proof of Property 4. Consider the generalized constitutive law for the full Cosserat model derived in [2, §6.3]. The reduced Lagrangian density in $\mathfrak{se}(3)$ per unit of deformed volume (for all configurations)[1] for a configuration $\mathcal{B}$ is given by $\mathfrak{L} = \mathfrak{T} - \mathfrak{U}$ [2] where $\mathfrak{T}, \mathfrak{U}$ respectively denote the volume's left-reduced kinetic and elastic potential energy densities in $\mathcal{B}$. From the Euler-Lagrange equation, we have

$$\tau_n = \frac{d}{dt}\frac{\partial \mathfrak{T}}{\partial \dot{\xi}_n} - \frac{\partial \mathfrak{T}}{\partial \xi_n} + \frac{\partial \mathfrak{U}}{\partial \eta_n}, \quad n = 1,\dots,N. \tag{13}$$

Suppose that the material mid-surface crosses the microstructures $\mathcal{M}_n$ which correspond to the mass center, then the kinetic energy density per unit of deformed area and its rate of change w.r.t ξ are [2]

$$\mathfrak{T}(\xi) = \frac{1}{2}\left\langle\begin{pmatrix}\omega \\ \nu, \end{pmatrix}, \begin{pmatrix}\bar{I}\omega \\ \bar{\rho}\nu\end{pmatrix}\right\rangle \tag{14}$$

$$\mathfrak{T}(\dot{\xi}) = \frac{1}{2}\left\langle\begin{pmatrix}\dot{\omega} \\ \dot{\nu}, \end{pmatrix}, \begin{pmatrix}\bar{I}\dot{\omega} \\ \bar{\rho}\dot{\nu}\end{pmatrix}\right\rangle \tag{15}$$

---

[1]Note that the full Lagrangian density of the soft multisection manipulator is $L_m = \int_0^L \mathfrak{L}(\boldsymbol{g}, \eta, \xi) dX$.

where $\bar{\rho}$ and $\bar{I}$ respectively denote the mass and angular inertia density per unit volume. It follows that

$$\partial_\xi \mathfrak{T} = \left(\begin{array}{c} \bar{I}\omega \\ \bar{\rho}\nu \end{array} \right), \quad \partial_{\dot{\xi}} \mathfrak{T} = \left(\begin{array}{c} \bar{I}\dot{\omega} \\ \bar{\rho}\dot{\nu} \end{array} \right). \tag{16}$$

In a similar vein, the left invariant density of internal energy $\mathfrak{U}$ is [3]

$$\mathfrak{U}(\eta) = \langle \mathcal{F}_{int}, (\eta - \eta^d) \rangle \tag{17}$$

for a desired η^d and field of internal force constraints $\mathcal{F}_{int} : X \in [0, L] \to \mathcal{F}_{int}(X) \in \mathfrak{se}(3)$. The potential energy per unit of metric area of the deformed surface (assuming that it is concentrated in the mid-surface) is [2]

$$\partial_\eta \mathfrak{U} = \left(\begin{array}{c} \partial \mathfrak{U}/\partial\gamma \\ \partial \mathfrak{U}/\partial\varepsilon \end{array} \right) - \left(\begin{array}{c} 0 \\ \varepsilon \end{array} \right) \mathfrak{L} \tag{18}$$

so that the Euler-Lagrange equation (13) becomes

$$\left(\begin{array}{c} \bar{I}\ddot{\omega} + \dot{\bar{I}}\dot{\omega} \\ \bar{\rho}\ddot{\nu} + \dot{\bar{\rho}}\dot{\nu} \end{array} \right) - \left(\begin{array}{c} \bar{I}\omega \\ \bar{\rho}\nu \end{array} \right) + \left(\begin{array}{c} \partial \mathfrak{U}/\partial\gamma \\ \partial \mathfrak{U}/\partial\varepsilon \end{array} \right) - \left(\begin{array}{c} 0 \\ \varepsilon \end{array} \right) \mathfrak{L}. \tag{19}$$

Observe: Under the PCS assumption, each microsolid is fixed so that the energy density per unit section of metric volume is akin to that of a rigid body. The kinetic and potential energies for the PCS model per section n of $N-$sections can thus be written as

$$\mathfrak{T} = \frac{1}{2} \sum_{n=1}^{N} \left\langle \left(\begin{array}{c} {}^{n+1}\omega_n \\ {}^{n+1}\nu_n, \end{array} \right), \left(\begin{array}{cc} {}^{n+1}\bar{I}_n & {}^{n+1}\omega_n \\ {}^{n+1}\bar{\rho}_n & {}^{n+1}\nu_n \end{array} \right) \right\rangle \tag{20}$$

where ${}^{n+1}\omega_n$ is the angular velocity of section $n+1$ in the frame of section n, ${}^{n+1}\nu_n$ is the linear velocity of section $n+1$ in the frame of section n e.t.c. Similarly, the sectional potential energies are

$$\mathfrak{U}(\eta_n) = \sum_{n=1}^{N} \langle \{\mathcal{F}_{int}\}_n, (\eta_n - \eta_n^d) \rangle. \tag{21}$$

Thus, the kinetic and potential energy are each linear in configuration parameters so that

$$\mathfrak{T} = \sum_{n=1}^{N} \frac{\partial \mathfrak{T}}{\partial \Sigma_n} \Sigma_n = \sum_{n=1}^{N} \Gamma \mathfrak{T}_n \Sigma_n,$$

$$\mathfrak{U} = \sum_{n=1}^{N} \frac{\partial \mathfrak{U}}{\partial \Sigma_n} \Sigma_n = \sum_{n=1}^{N} \Gamma \mathfrak{U}_n \Sigma_n \tag{22}$$

where Σ_n is an inertial parameter, $\Gamma \mathfrak{T}_n$ is a function of $q, \dot{q}$ and $\Gamma \mathfrak{U}_n$ is a function of q. Using (22) and plugging (16) and (18) into (13), we conclude that the sectionalized piecewise Cosserat dynamics is also linear-in-the-inertial-parameters, given as $\tau(q) = Y(q, \dot{q}, \ddot{q})\Theta$, where $Y(q, \dot{q}, \ddot{q})$ is the matrix function of $q, \dot{q}, \ddot{q}$ and Θ is the matrix of parameters. $\square$

IV. MULTIVARIABLE CONTROL

We will control the robot's dynamics by exploiting the properties of §III.

Fig. 2. PD computed torque control block diagram.

A. Proportional-(Integral)-Derivative Control, Redux.

We first show that regarding the generalized torque $\tau(q)$ as a control input, $u(q, \dot{q})$, linear feedback laws are (almost) sufficient for attaining a desired joint configuration (without gravity compensation) in the control law.

Theorem 2 (Cable-driven Actuation). *For a set of gains K_D and K_p which are damping and positive diagonal matrices, the control law (without gravity/buoyancy compensation)*

$$u(q, \dot{q}) = -K_p \tilde{q} - K_D \dot{q} - F(q) \tag{23}$$

under a cable-driven actuation globally asymptotically stabilizes (GAS) system (4), *where $\tilde{q}(t) = q(t) - q^d$ is the joint error vector for a desired equilibrium point in space q^d.*

Proof. Without gravity, the term $N(q)\text{Ad}_{g_r}^{-1}\mathcal{G} = 0$. Let

$$\breve{C}(q, \dot{q}) = C_1(q, \dot{q}) + C_2(q, \dot{q})$$

and write (4) for an arbitrary control input $u(q)$ as

$$M(q)\ddot{q} = u(q, \dot{q}) + F(q) - \left[\breve{C}(q, \dot{q}) + D(q, \dot{q}) \right] \dot{q}. \tag{24}$$

Consider the Lyapunov candidate function

$$V(q) = \frac{1}{2} \dot{q}^\top M(q)\dot{q} + \frac{1}{2}\tilde{q}^\top K_p \tilde{q}. \tag{25}$$

Observe: $V(q) > 0 \ \forall \ \{q, q^d\} \setminus (q = q^d), \dot{q} \neq 0$; and $V(q) = 0 \ \forall \{q, q^d\}$ when $(q = q^d)$ and $\dot{q} = 0$ in the joint space. Differentiating $V(q)$ yields

$$\dot{V}(q) = \dot{q}^\top M(q)\ddot{q} + \frac{1}{2}\dot{q}^\top \dot{M}(q)\dot{q} + \tilde{q}^\top K_p \dot{\tilde{q}},$$

$$= \dot{q}^\top \left(u(q, \dot{q}) + F(q) - \left[\breve{C}(q, \dot{q}) + D(q, \dot{q}) \right] \dot{q} \right)$$

$$\quad + \frac{1}{2}\dot{q}^\top \dot{M}(q)\dot{q} + \tilde{q}^\top K_p \dot{q},$$

$$= \dot{q}^\top \left(u(q, \dot{q}) + F(q) - \left[\breve{C}(q, \dot{q}) + D(q, \dot{q}) \right] \dot{q} \right)$$

$$\quad + \tilde{q}^\top K_p \dot{q} + \dot{q}^\top \left[\frac{1}{2} \left(\dot{M}(q) - 2\breve{C}(q, \dot{q}) \right) + \breve{C}(q, \dot{q}) \right] \dot{q},$$

$$= \dot{q}^\top \left[u(q, \dot{q}) + F(q) + K_p \tilde{q} - D(q, \dot{q})\dot{q} \right] \tag{26}$$

where the last line follows from the skew symmetric property established in Remark 1. Suppose we choose the control law (23), then

$$\dot{V}(q) = -\dot{q}^\top \left[K_D + D(q, \dot{q}) \right] \dot{q} \leq 0 \tag{27}$$

if we choose K_D as a block diagonal matrix of positive gains since the drag term $D(q, \dot{q}) > 0$. Thus, we have that the potential function is decreasing if q is non-zero. However, asymptotic stability of trajectories as a result of the potential (Lyapunov) function candidate does not automatically follow since $\dot{V}(t)$ is not negative at $\dot{q} = 0$. That is, it is possible for the manipulator's joint space variable derivative $\dot{q} = 0$ when $q \neq q^d$.

To prove global asymptotic stability, suppose the domain $\Omega \subset D \in \mathbb{R}^{6N \times 6N}$ is the compact, positively invariant domain with respect to (4). Let $\mathcal{E}$ be the set of all $q \in \Omega$ where $\dot{V}$ is identically zero so that (27) implies that $\dot{q} = 0$ and $\ddot{q} = 0$. From (24), we must have

$$M(q)\ddot{q} + \left[\check{C}(q, \dot{q}) + D(q, \dot{q}) \right] \dot{q} = -K_p \tilde{q} - K_D \dot{q} \quad (28)$$

which implies that $0 = -K_p \tilde{q}$ and hence $\tilde{q} = 0$. If Υ is the largest invariant set of $\mathcal{E}$, then by LaSalle's invariance theorem [9], every solution starting in Ω approaches Υ as $t \to \infty$. Whence, the equilibrium is GAS. $\quad \square$

Corollary 1 (Fluid-driven actuation). *If the robot is operated without cables, and is driven with a dense medium such as pressurized air or water, then the term $F(q) = 0$ so that the control law*

$$u(q, \dot{q}) = -K_p \tilde{q} - K_D \dot{q} \quad (29)$$

globally asymptotically stabilizes the system.

Proof. The proof follows easily since $F(q) = 0$ in (26). $\quad \square$

Theorem 3 (Gravity/Buoyancy-Compensated Control). *Without gravity and/or buoyancy-compensation, there are parasitic disturbances and unmodeled parameters in (4) where an offset in the positional error $\tilde{q}$ at steady state may show up since we do not explicitly compensate for gravity and buoyancy.where the PD control law is not sufficient for driving the strain states to equilibrium. The following controller will achieve zero steady state convergence.*

$$u(q, \dot{q}) = -K_p \tilde{q} - K_D \dot{q} - F(q) - N(q) A d_{g_r}^{-1} \mathcal{G}. \quad (30)$$

Proof. From (4), write

$$M(q)\ddot{q} = u(q, \dot{q}) + F(q) + N(q)\mathrm{Ad}_{g_r}^{-1}\mathcal{G} \\ - \left[\check{C}(q, \dot{q}) + D(q, \dot{q}) \right] \dot{q}. \quad (31)$$

Let us choose the Lyapunov function candidate

$$V(q) = \frac{1}{2}\dot{q}^\top M(q)\dot{q} + \frac{1}{2}\tilde{q}^\top K_p \tilde{q} + \frac{1}{2}\int_0^t \tilde{q}^\top(s) K_I \tilde{q} ds, \quad (32)$$

where $V(q) > 0 \; \forall \; \{q, q^d\} \setminus (q = q^d), \dot{q} \neq 0$; $V(q) = 0 \; \forall \{q, q^d\}$ when $(q = q^d)$, K_I is the block diagonal integral gain, and $\dot{q} = 0$ in the joint space. Tt can be verified that

$$\dot{V}(q) = \dot{q}^\top \left[u(q, \dot{q}) + F(q) + \left\{ K_p + \frac{K_I}{s} \right\} \tilde{q} \right. \\ \left. - D(q, \dot{q})\dot{q} + N(q)\mathrm{Ad}_{g_r}^{-1}\mathcal{G} \right] \quad (33)$$

where we have used the frequency domain representation of the integral operator i.e. $1/s$. If we set

$$u(q, \dot{q}) = - \left\{ K_p + \frac{K_I}{s} \right\} \tilde{q} - K_D \dot{q} - F(q) - N(q)\mathrm{Ad}_{g_r}^{-1}\mathcal{G}, \quad (34)$$

we must have

$$\dot{V}(t) = -\dot{q}^\top \left[K_D + D(q, \dot{q}) \right] q \leq 0, \text{ if } \dot{q} \neq 0 \quad (35)$$

else for $\dot{V}$ identically zero, LaSalle's principle applies. $\quad \square$

Suppose that we choose appropriate proportional and derivative gains with the gravity-compensation term in (34), then the integral again K_I may be ignored as

$$u(q, \dot{q}) = -K_p \tilde{q} - K_D \dot{q} - F(q) - N(q)\mathrm{Ad}_{g_r}^{-1}\mathcal{G}. \quad (36)$$

The proof of the theorem follows as a result.

V. NUMERICAL SETUP AND RESULTS

Our goal is to regulate the strain and strain velocity states of the robot per section under different constant tip loads *despite the inevitable non-constant loads due to gravity, external forces, and inertial forces.*

A. System Setup and Parameters

As seen in Fig. 1, the tip load acts on the $+y$-axis in the robot's base frame. We use $\mathcal{F}_p^y$ to represent the tip load acting along the $+y$ direction in what follows. Given the geometry of the robot, we choose a drag coefficient of 0.82 (a Reynolds number of order 104) for underwater operations. We set the Young's modulus, $E = 110kPa$ and the shear viscosity modulus to $3kPa$. The bending second inertia momenta are set to $I_y = I_z = \pi r^4/4$ while the torsion second moment of inertia is set to $I_x = \pi r^4/2$ for $r = 0.1m$, the arm's radius – uniform across sections. The arm length is $L = 0.2m$. We assume a (near-incompressible) rubber material makes up the robot's body and set its Poisson ratio to 0.45; the mass is chosen as $\mathcal{M} = \rho[I_x, I_y, I_z, A, A, A]$ for a cylindrical soft shell's nominal density of $\rho = 2,000kgm^{-3}$ as used in [17]; the cross-sectional area $A = \pi r^2$ so that $I_x = \pi r^4/2$. The drag screw stiffness matrix D in (4) is a function of each section's geometry and hydrodynamics so that $D = -\rho_w \nu^T \nu \check{D}\nu/|\nu|$ where ρ_w is the water density set to $997kg/m^3$, and $\check{D}$ is the tensor that models the geometry and hydrodynamics factors in the viscosity model (see [17, §II.B, eq. 6]). The curvilinear abscissa, $X \in [0, L]$ was discretized into 41 microsolids per section.

B. Discussion

We adopted the recursive articulated-body algorithm [7] and integrate the right-hand-side of differential equations (24) and (31) using a Runge-Kutta-Fehlberg (RKF) adaptive scheme implemented in Python and Torch [14] with relative and absolute errors respectively set to 10^{-7} and 10^{-9}. We have found these tolerance values to be crucial for a successful numerical integration scheme as it avoids
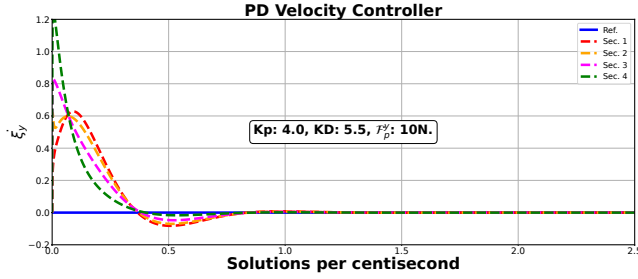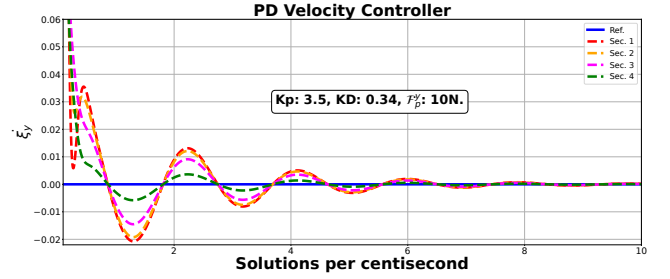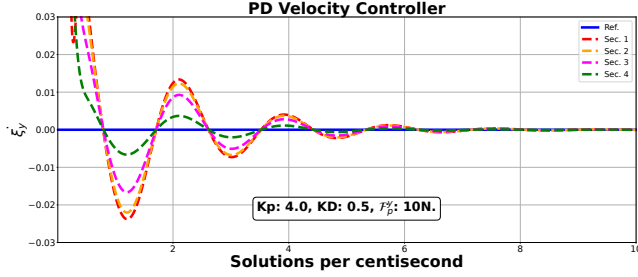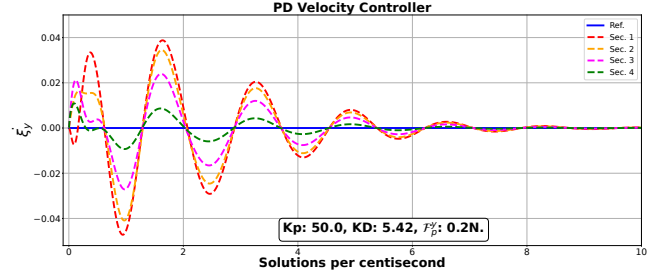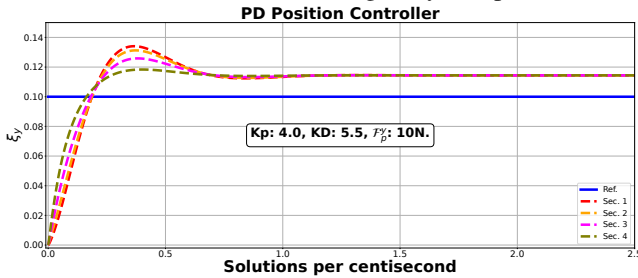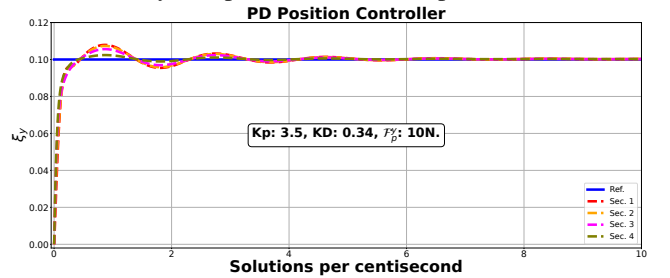
a1) Cable-driven, strain twist setpoint terrestrial control.

a2) Fluid-actuated, strain twist setpoint terrestrial control.

a3) Fluid-actuated, strain twist setpoint underwater control.

a4) Cable-driven, strain twist setpoint regulation.

b1) Position control with no gravity-compensation.

b2) Gravity-compensated terrestrial position control.

Fig. 3. *(a1 − a3):* Linear strain twist state regulation for a 4-section (41 microsolid pieces per section) soft arm under a $10N$ lateral tip load, $\mathcal{F}_p^y$ that is *(a1)* cable-driven in a sparse medium *(a2)* fluid-actuated in a sparse medium. *(a3)* fluid-actuated in a dense medium such as water (i.e. with drag forces compensation). *(a4)* Under a miniature tip-load of $0.2N$, a cable-driven 4-section arm finely regulates strain twists to equilibrium over time. *(b1-b2):* Linear strain position regulation for a cable-driven arm operating in air *(b1)* and a fluid-actuated arm illustrating the effect of steady state errors in the absence of gravity compensation. The horizontal axes show the number of (re-)integration time-steps per second for the adaptive Runge-Kutta-Fehlberg integrator we utilized in computing the controllers.

numerical instability. Depicted on the vertical axes of each chart of Fig. 3 are the strain positions or twists along $+y$-direction (on the robot's local frame) while the horizontal axes depict the number of adaptive RKF (re-) integration steps per for every tenth of a second. The trajectory evolution over time per discretized Cosserat section is shown in the various "dash-dotted" lines, while the "solid blue" lines denote the reference. The controller parameters are annotated within chart together with the amount of constant tip load in Newtons. We see that all joint configurations are stabilized to reference strain twist states $(\dot{q}^d)$ for respective constant tip loads. It can also be inferred that more sections a in the discretized Cosserat model lead to less bumpy state regulation strategy.

In *(a1−a3)*, the strain twists are precisely regulated to zero offset errors despite large constant tip loads *(a1-a3)*; and with small tip disturbances *(a4)*. Notably, the large value of the proportional gain causes overdamping in the transients

before convergence. However, a 20% error offset at steady state is observed in the linear strain position regulation case **(b1)** in the absence of the gravity compensation term in the control law. We attribute this to the nature of PD Lagrangian controllers realized via computed torque methods [19]. For accurate position control with PD controllers, steady state errors can be achieved when the gravity os compensated in the control design as *(b2)* shows.

VI. ACKNOWLEDGMENT

REFERENCES

[1] Gunjan Agarwal, Nicolas Besuchet, Basile Audergon, and Jamie Paik. Stretchable Materials for Robust Soft Actuators Towards Assistive Wearable Devices. *Scientific reports*, 6(1):34224, 2016. 1

[2] Frederic Boyer and Federico Renda. Poincaré's Equations for Cosserat Media: Application to Shells. *Journal of Nonlinear Science*, 27(1):1–44, 2017. ISSN 14321467. 3, 4

[3] Frederic Boyer, Mathieu Porez, and Alban Leroyer. Poincaré–cosserat equations for the lighthill three-dimensional large amplitude elongated body theory: application to robotics. *Journal of Nonlinear Science*, 20:47–79, 2010. 4

[4] Frédéric Boyer, Vincent Lebastard, Fabien Candelier, Federico Renda, and Mazen Alamir. Statics and Dynamics of Continuum Robots based on Cosserat Rods and Optimal Control Theories. *IEEE Transactions on Robotics*, 39(2):1544–1562, 2022. 1

[5] Eulalie Coevoet, Adrien Escande, and Christian Duriez. Optimization-based Inverse Model of Soft Robots with Contact Handling. *IEEE Robotics and Automation Letters*, 2(3):1413–1419, 2017. 1

[6] Eugène Maurice Pierre Cosserat and François Cosserat. *Théorie des corps déformables*. A. Hermann et fils, 1909. 1

[7] Roy Featherstone. *Rigid Body Dynamics Algorithms*. Springer, 2014. 5

[8] Michael W Hannan and Ian D Walker. Kinematics and the Implementation of an Elephant's Trunk Manipulator and other Continuum Style Robots. *Journal of Robotic Systems*, 20(2):45–63, 2003. 1

[9] Hassan K Khalil. *Nonlinear Control*, volume 406. Pearson New York, 2015. 5

[10] Cecilia Laschi, Matteo Cianchetti, Barbara Mazzolai, Laura Margheri, Maurizio Follador, and Paolo Dario. Soft robot arm inspired by the octopus. *Advanced robotics*, 26(7):709–727, 2012. 1

[11] Mariangela Manti, Taimoor Hassan, Giovanni Passetti, Nicolò D'Elia, Cecilia Laschi, and Matteo Cianchetti. A Bioinspired Soft Robotic Gripper for Adaptable and Effective Grasping. *Soft Robotics*, 2(3):107–116, 2015. 1

[12] Andrew D Marchese, Cagdas D Onal, and Daniela Rus. Autonomous Soft Robotic Fish Capable of Escape Maneuvers Using Fluidic Elastomer Actuators. *Soft robotics*, 1(1):75–87, 2014. 1

[13] R. W. Nuckols, S. Lee, K. Swaminathan, D. Orzel, R. D. Howe, and C. J. Walsh. Individualization of exosuit assistance based on measured muscle dynamics during versatile walking. *Science Robotics*, 6(60): eabj1362, 2021. 1

[14] Adam Paszke, Sam Gross, Francisco Massa, Adam Lerer, James Bradbury, Gregory Chanan, Trevor Killeen, Zeming Lin, Natalia Gimelshein, Luca Antiga, Alban Desmaison, Andreas Kopf, Edward Yang, Zachary DeVito, Martin Raison, Alykhan Tejani, Sasank Chilamkurthy, Benoit Steiner, Lu Fang, Junjie Bai, and Soumith Chintala. Pytorch: An imperative style, high-performance deep learning library. In *Advances in Neural Information Processing Systems 32*, pages 8024–8035. Curran Associates, Inc., 2019. 5

[15] Panagiotis Polygerinos, Zheng Wang, Kevin C Galloway, Robert J Wood, and Conor J Walsh. Soft robotic glove for combined assistance and at-home rehabilitation. *Robotics and Autonomous Systems*, 73: 135–143, 2015. 1

[16] Ke Qiu, Jingyu Zhang, Danying Sun, Rong Xiong, Haojian Lu, and Yue Wang. An efficient multi-solution solver for the inverse kinematics of 3-section constant-curvature robots. *arXiv preprint arXiv:2305.01458*, 2023. 1

[17] Federico Renda, Frédéric Boyer, Jorge Dias, and Lakmal Seneviratne. Discrete cosserat approach for multi-section soft manipulator dynamics. *IEEE Transactions on Robotics*, 34(6):1518–1533, 2018. 1, 2, 3, 5

[18] José Guadalupe Romero, Romeo Ortega, and Ioannis Sarras. A globally exponentially stable tracking controller for mechanical systems using position feedback. *IEEE Transactions on Automatic Control*, 60(3):818–823, 2014. 3

[19] Mark W. Spong. An historical perspective on the control of robotic manipulators. *Annual Review of Control, Robotics, and Autonomous Systems*, 5:1–31, 2022. 6

[20] Thomas George Thuruthel, Egidio Falotico, Federico Renda, and Cecilia Laschi. Model-based Reinforcement Learning for Closed-loop Dynamic Control of Soft Robotic Manipulators. *IEEE Transactions on Robotics*, 35(1):124–134, 2018. 1

[21] Hong Kai Yap, Nazir Kamaldin, Jeong Hoon Lim, Fatima A Nasrallah, James Cho Hong Goh, and Chen-Hua Yeow. A Magnetic Resonance Compatible Soft Wearable Robotic Glove for Hand Rehabilitation and Brain Imaging. *IEEE transactions on neural systems and rehabilitation engineering*, 25(6):782–793, 2016. 1